Mechanical Properties of TiO2 nanotubes investigated by AFM and FEM

Ji Zhou
Hunan University of Science and Engineering
Zuozhang Wang
Xiangtan University
Yunhong Jiang
Xiangtan University
Zhongmei Yang
Xiangtan University
Qiong Tian
Hunan University of Science and Engineering
Yanhuai Ding (yhding@xtu.edu.cn)
Xiangtan University https://orcid.org/0000-0003-1176-6397

Research Article

Keywords:

DOI: https://doi.org/10.21203/rs.3.rs-36131/v1

Abstract

The mechanical measurements of nanostructures are crucial to the development and processing of novel nanodevices. Herein, TiO2 nanotubes were synthesized from an electrospun method combined with subsequent heat-treatment. The elastic modulus and fracture strength of a single TiO2 nanotube were measured by atomic force microscopy (AFM). The effect of elastic modulus and dimensional size on the mechanical behaviors of the nanotubes was simulated by the finite element method (FEM).

1. Introduction

The design and construction of nanodevices such as microbatteries, quantum cascade

lasers, field-effect transistors, light-emitting diodes, gas nanosensors, etc. rely critically on our ability to fabricate functional heterostructures and interfaces with desirable characteristics [1-3]. Fortunately, the development of nanomaterials has created great excitement and expectations in the field of nanodevices. Much progress in the synthesis, fabrication and assembly of nanomaterials has already been gained in the past decades. Especially, nanostructured semiconducting oxides have attracted much attention due to their tunable physical properties and wide applications. Various kinds of semiconducting oxides, such as TiO_2 [4], ZnO [5], SiO_2 [6], In_2O_3 [7], Ga_2O_3 [8], GeO_2

[9], SnO_2 [10], CdO [11], and PbO_2 [12] with different morphology have been

successfully prepared. Among them, TiO_2 has been investigated mainly owing to its

widespread applications in lithium ion batteries [13], solar cells [14], photocatalysts

[15], and sensors [16]. Most of the previous researches focused on the morphological controlling and property modulation of TiO_2. The mechanical behavior of materials at

the nanoscale is often different from that at the macroscopic scale. Thus, the mechanical properties of nanomaterials are crucial to the development and processing of novel nanodevices [17, 18].

The challenge of research on nanomechanical properties is not only due to the lack of nanoscale experimental techniques, but also the lack of multiscale theories to describe the size effects [19]. In recent years, in-situ transmission electron microscopy (TEM) and scanning electron microscopy (SEM) nanomechanical testing have been developed to image and measure the deformation inside the instruments [20-22]. Besides, atomic force microscopy (AFM) was employed to image and measure the deformation and applied force of the object simultaneously at the nanoscale [23-26]. As an open platform, AFM provides multiple possibilities for the mechanical characterization of nanomaterials. For example, the three-point bending test and nanoindentation were widely performed on AFM to measure Young's modulus and hardness of nanostructures [24, 27, 28]. However, due to the lack of basic data and related experimental equipment, the finite element method (FEM) was widely employed to simulate and

predict the mechanical properties of nanomaterials under complicated conditions[10, 25, 26, 29]. Herein, TiO_2 nanotubes were synthesized from an

electrospun method combined with subsequent heat-treatment. A series of destructive and non-destructive tests were carried out to characterize the mechanical properties of a single TiO_2 nanotube. The fracture strength of a single TiO_2 nanotube was measured by

the AFM technology. The effect of elastic modulus and dimensional size on the

mechanical behaviors of the nanotubes was simulated by the FEM.

2. Experimental

2.1 Preparation of materials

TiO_2 nanotubes were synthesized from an electrospun method combined with subsequent heat-treatment [30]. In a typical procedure, a certain amount of polyvinyl Pyrrolidone (PVP, M_W1300000), acetic acid and titanium tetraisopropanolate were dissolved in ethanol. The as-prepared solution and mineral oil were used as external and internal fluid in coaxial electrospinning. The distance (from the tip of the pinhead to the collector: 20 cm) and the electrospun voltage (applied to the tip: 15kV) were fixed. The obtained electrospun membrane was soaked in n-octane to remove the mineral oil. After being heat-treated at 500°C for 3h, TiO_2 nanotubes were fabricated from the electrospun membrane.

2.2 Characterization of materials

Morphology of TiO_2 nanotubes was observed by field emission scanning electron microscope (FEI Nova NanoSEM450), transmission electron microscope (FEI Tecnai G2 F30) and atomic force microscopy (Bruker Multimode 8). Powder XRD measurements were performed on a Bruker D8 Advance Powder X-ray diffractometer using CuKα (λ = 0.15406 nm) radiation. For nanomechanical characterization, TiO_2 nanotubes were ground and then dispersed in ethanol. One drop of the dispersion was deposited on the surface of a Si wafer. The morphology and location were confirmed by AFM under Peak-Force Quantitative Nanomechanics (PFQNM) mode. The fracture strength was measured by using nanoindentation mode. The mechanical behavior of the

nanotubes was simulated by FEM. More details about the FEM simulation were provided in Supporting Information.

3. Results And Discussion

Fig.1a exhibits the low magnification SEM image of TiO_2nanotubes. Large quality of TiO_2 nanotubes with various diameters was observed. The diameter of the TiO_2 nanotubes was in the range of 30~200nm. The tube-like structure was confirmed by the fractured surface. The detailed structure of the

synthesized TiO_2 nanotubes was studied by TEM. The clear tube wall can be recognized in Fig.2b. The HRTEM image (Fig.1c) indicates that TiO_2 nanotube apparently consists of tiny nanocrystallites, indicating a polycrystalline nature of the nanotubes. XRD patterns (Fig.1d) reveal that the presence of the crystallographic structure of anatase was observed for the sample calcined at 500°C [31].

Morphology of a single TiO_2 nanotube before and after nanoindentation was presented in Fig.2. The size of the TiO_2 tube tested by AFM was presented in S1. A well-shaped TiO_2 nanotube with a diameter of 220 nm was picked as a target (Fig.2a). The AFM nanoindentation test was performed after surface scanning. The AFM tip was carefully moved to the top of the nanotube by repeatedly zooming in [32]. Then a controllable force was exerting to the AFM tip until the nanotube was broken (Fig.2b). Apparently, the TiO_2 nanotube shows brittle fracture behavior at nanoscale. At the fracture location, the wall thickness of the nanotube can be measured. After the nanoindentation test, the mechanical properties of the nanotube were calculated from the force-distance curve collected by the AFM.

A typical force-displacement curve obtained from the nanoindentation test is shown in Fig.3. The force-displacement curve can be divided into three stages: in the first stage, the indentation force linearly increased with the displacement, indicating the elastic deformation region of the nanotube. In the second stage, the indenter impaled the wall of the nanotube. No apparent plastic deformation was observed, indicating a brittle fracture of the nanotubes. In the third stage, with the further increase of the indentation force, the destruction continued until the complete collapse of the nanotube. The fracture strength of the single TiO_2 nanotube measured by AFM is ~ 35GPa. Based on the AFM experiments, the FEM model was established as shown in S2. The effect of elastic modulus and dimensional size on the mechanical behaviors of the nanotubes can be predicted by FEM simulation. A typical deformation nephogram from FEM simulation is shown in S3. Obviously, the maximal value of the deformation can be found under the indenter. Furthermore, most of the deformation appears at the top surface of the tube.

The effect of the equivalent radius of the indenter on the deformation of the TiO_2 nanotubes over the linearly elastic range was simulated by FEM as shown in Fig.4a. Undoubtedly, with the decrease of the equivalent radius of the indenter, the deformation of the TiO_2 nanotubes under the same force increases. It should be noticed that this phenomenon becomes increasingly obvious with the decrease in the equivalent radius. Besides, with the indent force increases, the deformation increases linearly. Slight difference in the slopes is found, indicating the effect of different equivalent radius on the deformation of TiO_2 nanotubes is exhibited in different ways.

With a fixed indented force, smaller the equivalent radius, larger the nanotube's

deformation due to the remarkably increasing pressure under the indenter. As shown in Fig.4b, with the radius is in the range of 0.02 - 0.03 μm, the effect of the radius on the deformation can be neglected.

Fig.6 Effect of the dimensional size of the nanotubes. (a) Relationship between indented force and deformation with fixed L/D. (b) Effect of L/D on the deformation of nanotubes with certain indented

force.

4. Conclusions

In summary, the mechanical behavior of a single TiO_2 nanotube was successfully characterized by AFM and FEM method. The ultimate strength of the TiO_2 nanotube measured from AFM is around 35 GPa. FEM results indicate that the mechanical behavior of the nanotubes is greatly affected by the indenter's equivalent radius, material's elastic modulus and nanotube's dimensional size. Based on the FEM simulation, the mechanical behavior of the nanotubes can be effectively predicted.

Declaration

Funding

This work was financially supported by National Natural Science Foundation of China (No. 51002128) and Scientific Research Foundation of Hunan Provincial Education Department (No.17A205).

Conflicts of interest

The authors declare no competing financial interest

References

1. Wang ZL. Nanobelts, nanowires, and nanodiskettes of semiconducting oxides—from materials to nanodevices. *Adv Mater* 2003, **15**: 432-436.
2. Zhang Q, Li H, Gan L, *et al.* In situ fabrication and investigation of nanostructures and nanodevices with a microscope. *Chem Soc Rev* 2016, **45**: 2694-2713.
3. Yang Z, Jiang Y, Zhang W, *et al.* Solid-state, low-cost, and green synthesis and robust photochemical hydrogen evolution performance of ternary TiO_2/$MgTiO_3$/C photocatalysts. *iScience* 2019, **14**: 15-26.
4. Yang Z, Jiang Y, Yu Q, *et al.* Facile preparation of exposed {001} facet TiO_2 nanobelts coated by monolayer carbon and its high-performance photocatalytic activity. *Mater Sci* 2017, **52**: 13586-13595.
5. Ren H, Ding Y, Jiang Y, *et al.* Synthesis and properties of ZnO nanofibers prepared by electrospinning. *J Sol-Gel Sci Technol* 2009, 52: 287-290.
6. Dahlberg KA, Schwank JW. Synthesis of Ni@SiO_2 nanotube particles in a water-in-oil microemulsion template. *Chem Mater* 2012, **24**: 2635-2644.
7. Liang CH, Meng GW, Lei Y, et al. Catalytic growth of semiconducting In_2O_3 nanofibers. *Adv Mater* 2001, **13**: 1330-1333.
8. Kim J, Oh S, Mastro MA, *et al.* Exfoliated β-Ga_2O_3 nano-belt field-effect transistors for air-stable high power and high temperature electronics. *Phys ChemChem Phys* 2016, **18**: 15760-15764.

9. Li X, Liang J, Hou Z, *et al.* Coordination complex pyrolyzation for the synthesis of nanostructured GeO_2 with high lithium storage properties. *Chem Commun* 2014, **50**: 13956-13959.
10. Liu X, Li K, Duan X, *et al.* Mechanical properties of individual core-shell-structured SnO_2@C nanofibers investigated by atomic force microscopy and finite element method. *Sci China Technol Sci* 2018, **61**: 1144-1149.
11. Sonawane NB, Baviskar PK, Ahire RR, *et al.* CdO necklace like nanobeads decorated with pbs nanoparticles: Room temperature lpg sensor. *Mater Chem Phys*
12. 2017, **191**:168-172.
13. Moncada A, Piazza S, Sunseri C, *et al.* Recent improvements in PbO_2 nanowire electrodes for lead-acid battery. *J Power Sources*, 2015, **275**: 181-188.
14. Ding Y-H, Zhang P, Ren H-M, *et al.* Preparation of graphene/TiO_2 anode materials for lithium-ion batteries by a novel precipitation method. *Mater Res Bull* 2011, **46**: 2403-2407.
15. Kogo A, Sanehira Y, Numata Y, *et al.* Amorphous metal oxide blocking layers for highly efficient low-temperature brookite TiO_2-based perovskite solar cells. *ACS ApplMater & Interf* 2018, **10**: 2224-2229.
16. Jiang Y, Yang Z, Zhang P, *et al.* Natural assembly of a ternary Ag–SnS–TiO_2 photocatalyst and its photocatalytic performance under simulated sunlight. *RSC Adv* 2018, **8**: 13408-13416.
17. Zalduendo MM, Langer J, Giner-Casares JJ, *et al.* Au nanoparticles–mesoporous tio2 thin films composites as sers sensors: A systematic performance analysis. *J PhysChem C*, 2018, **122**: 13095-13105.
18. Rao CNR, Cheetham AK. Science and technology of nanomaterials: Current status and future prospects. *J Mater Chem* 2001, **11**: 2887-2894.
19. Teo BK, Sun XH. From top-down to bottom-up to hybrid nanotechnologies: Road to nanodevices. *J Cluster Sci* 2006, **17**: 529-540.
20. Stampfer C, Helbling T, Jungen A, *et al.* Micromachined pressure sensors for electromechanical characterization of carbon nanotubes. *Phys Status Solidi b* 2006, **243**: 3537-3541.
21. Yu Q, Legros M, Minor AM. In situ TEM nanomechanics. *MRS Bull* 2015, **40**: 62-70.
22. Wang MS, Kaplan-Ashiri I, Wei XL, *et al.* In situ tem measurements of the mechanical properties and behavior of WS_2*Nano Research* 2008, **1**: 22
23. Allison PG, Moser RD, Schirer JP, *et al.* In-situ nanomechanical studies of deformation and damage mechanisms in nanocomposites monitored using scanning electron microscopy. *Mater Lett* 2014, **131**: 313-316.
24. Lee S-H, Tekmen C, Sigmund WM. Three-point bending of electrospun TiO_2 nanofibers. *Mater Sci Eng A*, 2005, **398**: 77-81.
25. Ding Y, Zhang P, Jiang Y, *et al.* Mechanical properties of nylon-6/sio2 nanofibers prepared by electrospinning. *Mater Lett* 2009, **63**: 34-36.

26. Jin H, Ding Y-H, Wang M, *et al.* Designable and dynamic single-walled stiff nanotubes assembled from sequence-defined peptoids. *Nat Commun* 2018, **9**: 270.
27. Li Z, Jiang X, Deng X, *et al.* Mechanical characterization of PMMA by AFM nanoindentation and finite element simulation. *Mater Res Express* 2016, **3**: 115302.
28. Liu X, Li Z, Jiang YH, *et al.* Mechanical properties of a single SnO_2 fiber prepared from the electrospinning method. *J Sol-Gel Sci Technol* 2017, **84**: 152-157.
29. Ding YH, Deng XH, Jiang X, *et al.* Nanoscale mechanical characterization of PMMA by afm nanoindentation: A theoretical study on the time-dependent viscoelastic recovery. *J Mater Sci* 2013, **48**: 3479-3485.
30. Hui C, Zheng L, Xing L, *et al.* Compressive mechanical properties of porous GO materials prepared from freeze-drying method. *Mater Res Express* 2017, **4**: 025601.
31. Jiang Y, Ding Y, Zhang P, *et al.* Temperature-dependent on/off PVP@TiO_2 separator for safe li-storage. *J Membrane Sci* 2018, **565**: 33-41.
32. Ren HM, Ding YH, Chang FH, *et al.* Flexible free-standing TiO_2/graphene/PVDF films as anode materials for lithium-ion batteries. *Appl Surf Sci* 2012, **263**: 54-57.
33. Shen W, Jiang B, Han BS, *et al.* Investigation of the radial compression of carbon nanotubes with a scanning probe microscope. *Phys Rev Lett* 2000, **84**: 3634-3637.

Figures

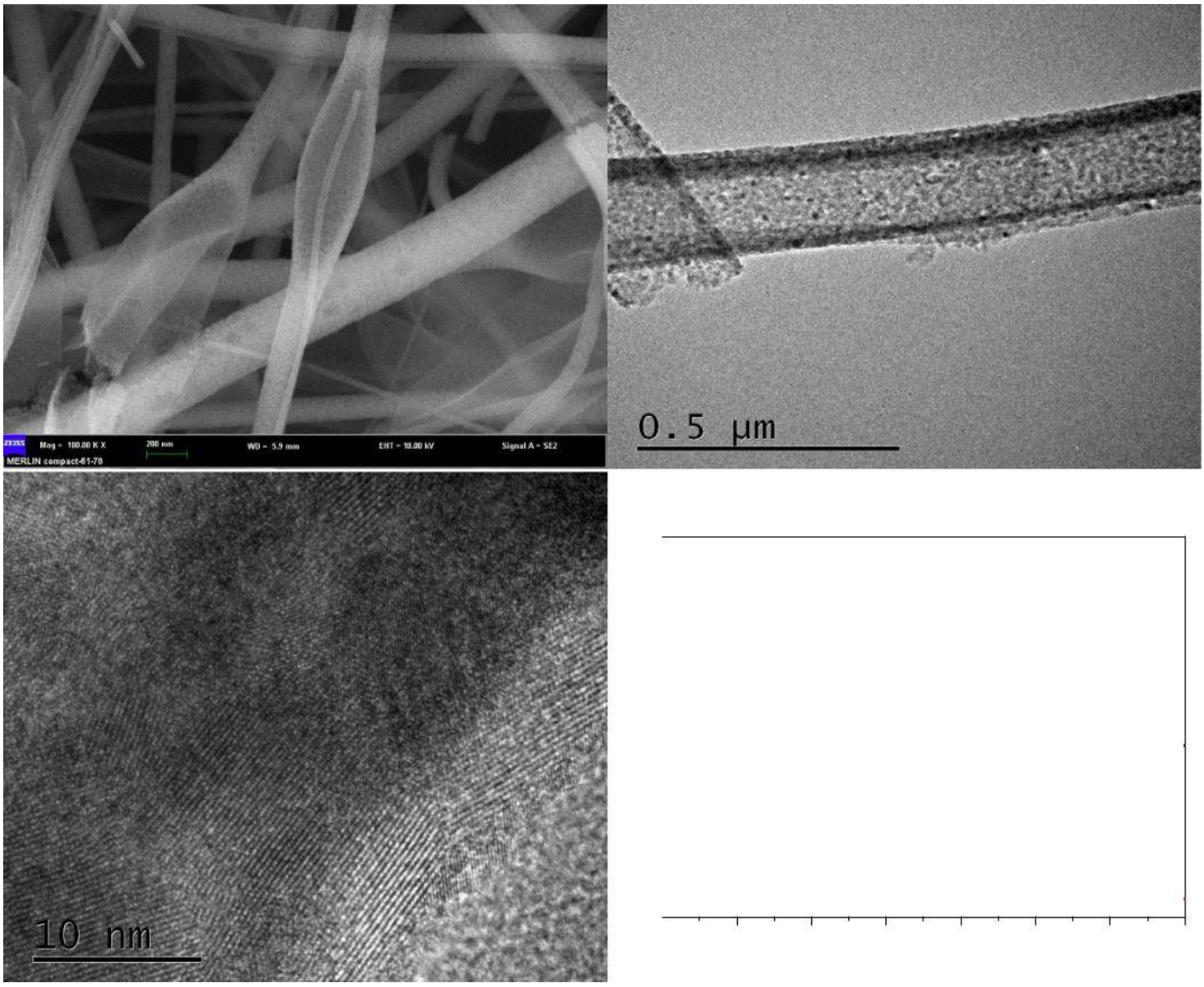

Figure 1

(a) SEM image, (b) TEM image, (c) HRTEM image and XRD patterns of TiO2 nanotube.

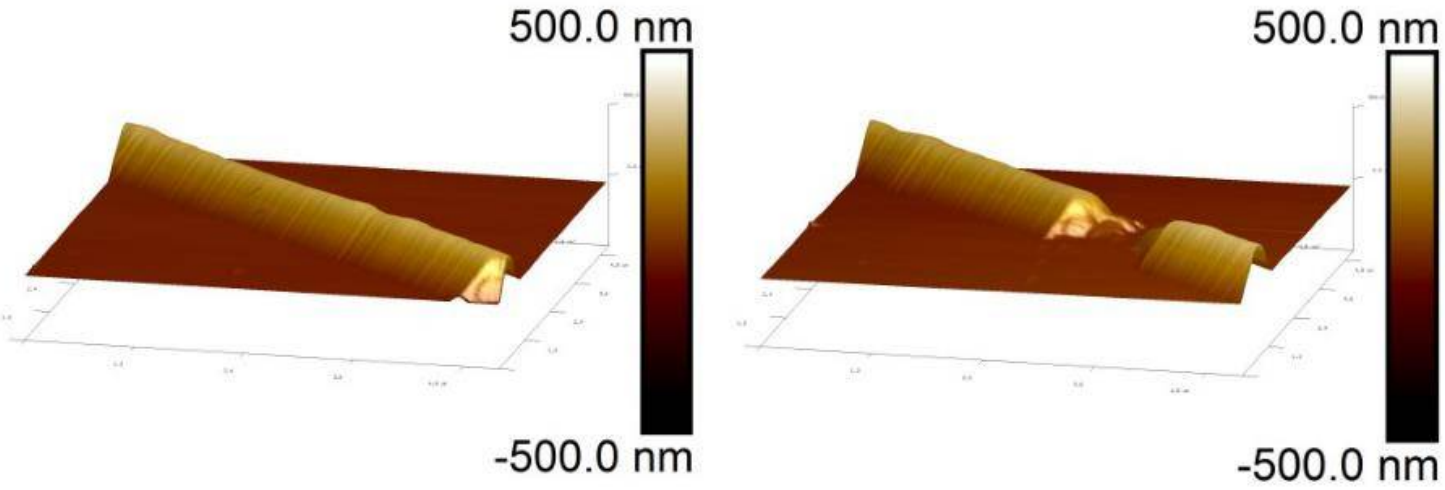

Figure 2

AFM image of a single TiO2 nanotube (a) before and (b) after nanoindentation.

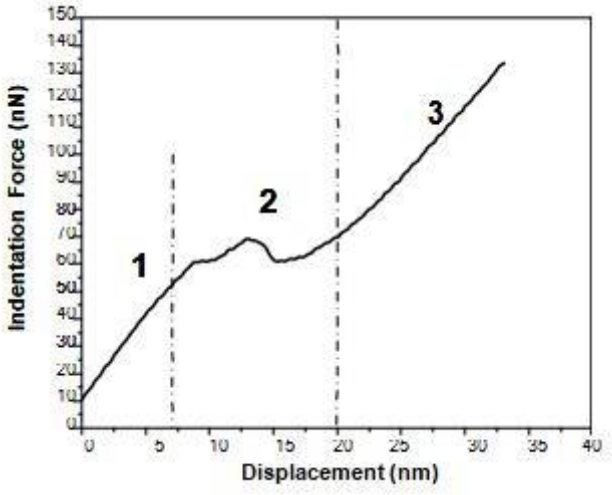

Figure 3

A typical force-displacement curve obtained from the nanoindentation test. The effect of the equivalent radius of the indenter on the deformation of the TiO2

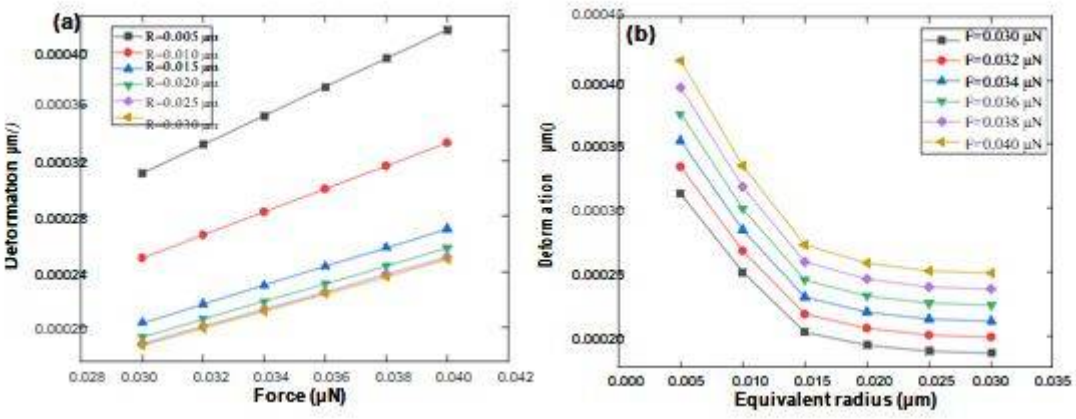

Figure 4

Effect of the equivalent radius of the indenter on the deformation of the TiO2 nanotubes simulated by FEM. (a) Relationship between the nanotube's deformation and the indented force. (b) Relationship between the nanotube's deformation and the equivalent radius.

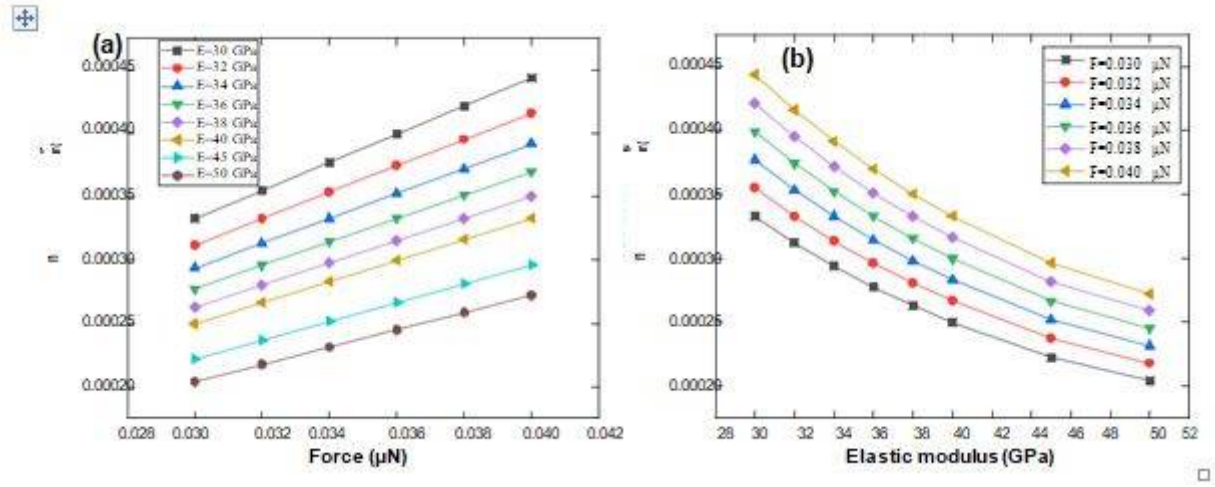

Figure 5

Relationship between nanotube's deformation and indented force (a) and elastic modulus (b) simulated by FEM.

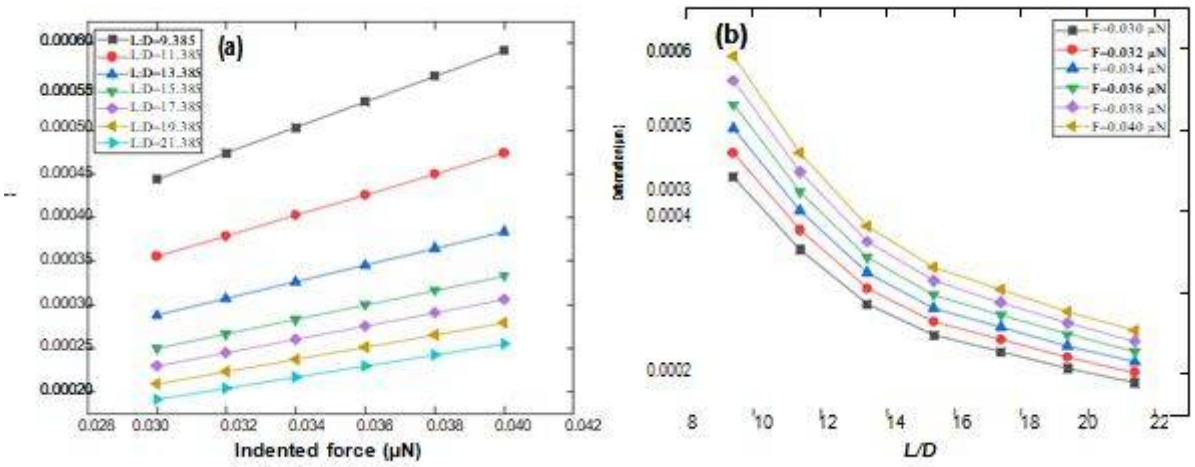

Figure 6

Effect of the dimensional size of the nanotubes. (a) Relationship between indented force and deformation with fixed L/D. (b) Effect of L/D on the deformation of nanotubes with certain indented force.

Supplementary Files

This is a list of supplementary files associated with this preprint. Click to download.

- Supplementry.docx